PAPER

A multiparametric model for the industrialization of co-precipitation synthesis of nano-commodities

View the article online for updates and enhancements.

IOP ebooks™

Bringing you innovative digital publishing with leading voices to create your essential collection of books in STEM research.

Start exploring the collection - download the first chapter of every title for free.

A multiparametric model for the industrialization of co-precipitation synthesis of nano-commodities

Lilian Celeste Alarcón Segovia[1]**, Jorge Ivan Daza Agudelo**[1]**,**
Romina Julieta Glisoni[2]**, Carlos Acha**[3] **, María Mercedes De Zan**[4] **and**
Ignacio Rintoul[1]

[1] Instituto de Desarrollo Tecnológico para la Industria Química, Universidad Nacional del Litoral and Consejo Nacional de Investigaciones Científicas y Técnicas, Santa Fe, Argentina
[2] Instituto de Nanobiotecnología. Departamento de Tecnología Farmacéutica, Cátedra de Tecnología Farmacéutica II, Facultad de Farmacia y Bioquímica, Universidad de Buenos Aires and Consejo Nacional de Investigaciones Científicas y Técnicas, Buenos Aires, Argentina
[3] Departamento de Física, FCEyN, Universidad de Buenos Aires e IFIBA, UBA-Conicet, Buenos Aires, Argentina
[4] Laboratorio de Control de Calidad de Medicamentos, Facultad de Bioquímica y Ciencias Biológicas, Universidad Nacional del Litoral, Santa Fe, Argentina

E-mail: irintoul@santafe-conicet.gov.ar

CrossMark

Abstract

Magnetite superparamagnetic nanoparticles (MNP) are becoming one of the firsts nanocommodity products. MNP find a number of applications and they are been produced at relatively large scale. The co-precipitation method presents many technical and economical advantages among alternative processes. However, the relationships between physical and chemical reaction conditions during the co-precipitation process and the resulting properties of obtained MNP are not yet fully understood. The novelty of this contribution is the establishment of the cross-dependency effects of the main physical and chemical parameters of the co-precipitation reaction on the properties of resulting MNP. The conditions were varied by following an experimental design. The crystallite size, particle size and magnetization of the MNP and the Z-potential and size of their aggregates were selected as main response properties. A set of equations in the form of 4D surface responses in the space of co-precipitation process variables was obtained and analyzed in terms of the resulting properties. The set of equations is useful to predict, optimize and tailor very precisely the properties of resulting MNP as a function of reaction conditions.

Keywords: industrialization, process optimization, chemical engineering, production of nanoparticles, nanomagnetite

(Some figures may appear in colour only in the online journal)

1. Introduction

Magnetite nanoparticles (MNP) present many interesting properties and have found a number of uses and potential applications in key technological fields. Lately, several comprehensive reviews have been published underling the emerging progress in the understanding of the relationships between geometrical, chemical, physical and biological properties of MNP with potential uses. In the field of medicine MNP were reviewed for targeting specific tissues [1–4], for diagnosis and medical imaging [4–9], for the treatment of iron related diseases [1, 3], for antimicrobial therapies [3, 10, 11], for drug delivery [2, 5, 8, 12–14], for hyperthermia treatments [4, 15], and for many other biomedical

applications [8, 16, 17]. In the field of environmental protection and remediation MNP are been explored for heavy metal removal [18] and enzyme carriers [19] in wastewater treatments and to detect environmental pollutants in new analytical techniques [20]. In the fields of building materials and chemical industry they are been used for enhancing the properties of cements and composites [21] and as industrial catalysts [22], respectively. And, very interestingly, in the field of sustainable energy production MNP are been proposed as material for electrochemical energy storage [23] and as enhancer of biological production of hydrogen [24].

The unquestionable progress in the knowledge of properties and the ever growing number of uses and potential new applications of MNP has pushed the scientific interest in tailoring their properties and structures through smart controlling of reaction conditions during the processes of syntheses [25]. Among several methods, the co-precipitation method is an extended method with many advantages. It is robust, cheap, easy to scale up and very extended for large industrial productions [26]. The chemical co-precipitation method consists in mixing ferrous and ferric salts in aqueous medium to form magnetite. Here, the conditions of synthesis greatly affect the geometrical, chemical and physical properties of resulting MNP [27].

The formation of MNP was demonstrated to progress within the framework of classical nucleation theory [28]. In this theory, temperature plays a crucial role. The effect of reaction temperature on the size of MNP has been extensively reported. For example, the size of MNP was found to increase from 3.8 to 10.9 nm when the temperature changed from 1 °C to 95 °C in a co-precipitation carried out at very high mixing strength. In these conditions, the temperature dependence of the size distribution was found to follow the terms of the Ostwald ripening [29]. Another study, reported the minimum size of MNP as 8 nm when synthesized at 45 °C in a co-precipitation carried out at medium mixing strength [30]. Higher and lower reaction temperatures promoted the synthesis of bigger MNP. Here, the temperature was proposed to alter the critical size, the extent of aggregation of growing nucleus and the degree of mobility and collisions of reacting species. Evidently, the degree of mixing also participates in the definition of resulting properties of MNP.

The effect of the degree of mixing on the size of MNP has been also extensively investigated [29, 30]. The increase of the stirring rate of reaction medium from 400 to 800 rpm was reported to decrease the size of MNP from 9.41 to 7.83 nm. This effect was explained in terms of the mechanical energy transferred to the reaction medium [31] and the reduction of the growth kinetics of nucleus through the enhancement of anomalous diffusion of species [32]. Additionally, MNP with sizes in the range between 8.9 and 12.5 nm were obtained by varying the mixing strength at room temperature [33]. And, ultrafast jet mixing was reported to promote stable nucleation and kinetics of grows useful to control the resulting particle size of MNP within 3.8–10.9 nm [29]. Finally, the effects of chemical recipe formulation such as the total iron content, the relative concentration of ferrous and ferric ions, the dissolved oxygen and the injection fluxes on the size and magnetic

properties of resulting MNP were reported [34]. It was found that stoichiometric 2:1 amounts of ferrous to ferric ions is optimal to obtain MNP and to avoid the apparition of other by-product iron oxides.

The size of MNP is extensively study because it is intrinsically related to their magnetic properties [30]. The smaller the size of MNP, the lower their saturation magnetization. Several authors explained this effect in terms of the surface/bulk order/disorder interactions and the geometrical irregularities of the nanoparticles [35–39].

In general, the literature reports the effects of reaction conditions on the size, magnetization and other key properties of obtained MNP by studies carried out following the one-factor-at-a-time method. It means to vary one parameter while keeping constant all the others. However, the variation of physical reaction parameters such as the temperature and the degree of mixing seems to be inherently related to the variation chemical reaction parameters such as pH, solubility of reacting species and the ratio of formation of between magnetite and other iron oxide by-products such as maghemite and hematite [36]. Therefore, it is important to develop a comprehensive model including both, physical and chemical reaction parameters, to predict the structure and properties of resulting MNP.

This work presents a comprehensive model to predict the size and the magnetization of MNP and the Z-potential and the size of MNP aggregates obtained by a chemical co-precipitation method. The model uses as inputs four key reaction parameters. The reaction temperature and the degree of mixing were selected as key physical reaction parameters. And the total iron content in the co-precipitating medium and the volume of base used as pH regulator were selected as key chemical reaction parameters. These four key parameters have been selected according to the common agreement found in the literature respect to the most influencing parameters on the resulting characteristics of MNP. It is important to mention that other parameters such stoichiometry of iron ions and pH are not considered since they were already optimized to avoid the apparition of iron oxide by-products. The experimental conditions were defined using to a Taguchi type experimental design [40].

A 4D surface response was built with the experimental results. The obtained set of equations is useful to predict the size and magnetization of MNP and the Z-potential and the size of MNP aggregates as functions of the key chemical and physical reaction parameters set during the chemical co-precipitation.

2. Experimental part

2.1. Materials

Ultrapure ferric chloride hexahydrate, $FeCl_3 \cdot 6H_2O$, (Biopack, Argentina), ultrapure ferrous chloride tetrahydrate, $FeCl_2 \cdot 4H_2O$, (Biopack, Argentina), ammonium hydroxide aqueous solution, NH_4OH, 28% w/w (Anedra, Argentina), ultrapure N_2 gas grade 4.5 (Indura, Argentina), Type 1 ultra-pure water with resistivity

of 18.2 MΩ and density $\delta_w = 0.99704$ g cm^{-3} and absolute methanol (Cicarelli, Argentina) were used as iron sources, pH regulator, non-oxidant atmosphere, reaction medium and swashing solvents, respectively. Glycerol (Cicarelli, Argentina) was used as dispersion medium of obtained nanoparticles.

2.2. Synthesis of MNP

MNP were synthesized using a co-precipitation method [41]. Firstly, an aqueous solution of FeCl$_3$·6H$_2$O and FeCl$_2$·4H$_2$O was prepared. The molar ratio between FeCl$_3$/FeCl$_2$ = 2. Secondly, the solution was put under stirring at certain speed and thermostatted at a defined temperature. Thirdly, a certain amount of NH$_4$OH 28% w/w solution was added to induce the precipitation of Fe$_3$O$_4$. The precipitation reaction was left to proceed during 60 min under N$_2$ atmosphere. The stirring speed and temperature were kept constant during all the experiment. The obtained dark precipitate was washed with deionized water to remove Cl$^-$ ions and the remaining NH$_4$OH. The sedimentation of the precipitate was assisted using strong neodymium magnets. Subsequently, the precipitate was washed with methanol and magnetically decanted again. And finally, it was vacuum dried for approximately 45 min and then stored in a hermetically sealed container.

The total iron content, the degree of mixing, the temperature and the amount of NH$_4$OH added to the iron solution were selected as synthesis variables.

2.3. Experimental design

The Taguchi method is commonly used to study processes with four interdependent parameters [42, 43]. The method proposes that the response (Y) to the stimuli of the simultaneous variation of four parameters (A, B, C, D) can be expressed as a polynomial function according to equation (1).

$$Y = \Sigma_{h,k,l,m} a_{h,k,l,m} A^h B^k C^l D^m. \tag{1}$$

The indexes h, k, l and m are non-negative integers going from 0 to ∞. Each term of the sum is composed by the product of an empirical coefficient ($a_{h,k,l,m}$) determined by a least squares fit and the variables powered to non-negative integer exponents. The higher the complexity of the response to a given stimuli, the higher are the exponents in the terms and the higher is the number of terms of the sum. The resulting polynomial function may has infinite terms and can, eventually, describe any functionality Y (A, B, C, D).

In the present contribution, the number of experiments was limited to nine. Therefore, nine experiments give the possibility to define a polynomial function of nine terms. The selection of the nine terms was carried out using experimental raw data and iterating using Minitab 17 software. Minitab 17 software is a mathematical software that solves equation systems easily.

The reaction parameters: A, B, C and D correspond to the total iron content in the solution, the temperature, the degree of mixing and the amount of base used to pH adjustment in the co-precipitating solution, respectively. Each variable was

Table 1. Experimental design.

| | Parameters | | | |
| | A | B | C | D |
Samples	Iron content (mol)	Temperature (°C)	Degree of mixing (rpm)	NH$_4$OH 28% (ml)
S1	0.034 50	30	1000	34
S2	0.017 25	70	1000	42
S3	0.069 00	50	1000	26
S4	0.069 00	70	500	34
S5	0.034 50	70	750	26
S6	0.034 50	50	500	42
S7	0.017 25	26	500	30
S8	0.069 00	42	750	30
S9	0.017 25	34	750	50

set at three different levels. Five responses were analyzed and correspond to the crystallite size (CS), the particle size (PS) and the maximum magnetization (M_{max}) of the MNP and the Z-potential (ZP) and size (AS) of their corresponding aggregates.

The responses were first studied in an attempt to find correlations among them and to minimize the number of surface responses. The selected responses for surface analysis resulted in 4D surfaces in the space of the mentioned variables. Subsequently, 2D plots were used to conclude and predict properties of resulting MNP to the simultaneous variation of their reaction conditions.

2.4. Synthesis conditions

Nine experiments with different conditions give the possibility to define a polynomial fit of nine terms. Here, the total iron content in the solution was set at 0.01725, 0.0345 and 0.069 mol. The degree of mixing was set at 500, 750 and 1000 rpm. The temperature was set at 30 °C, 50 °C and 70 °C. Finally, the amount of NH$_4$OH solution was set at 26, 34 and 42 ml. Table 1 presents the precipitation conditions according to the Taguchi L9 experimental design.

The amounts of NH$_4$OH used in the experiments were enough to saturate the pH at 12 in all cases. The variation of NH$_4$OH did not varied the pH level. The pH remained constant and equal to 12 during the co-precipitation reaction in all the experiments. High pH is important to avoid the formation of by-product iron oxides: maghemite and hematite.

2.5. Characterization

The obtained precipitates were characterized by x-ray diffraction (XRD), (x-ray Diffractometer Model XD-D1 Shimadzu, Japan) to analyze their purity, crystalline phase and the size of the ordered domains, also named as CS. The diffractometer operated with a Cu-Kα x-ray source with wavelength $\lambda = 1.54$ Å. The PS were measured using a high-resolution transmission electron microscope (TEM), (JEOL 100 CX II) operating at 100 kV and magnifications of
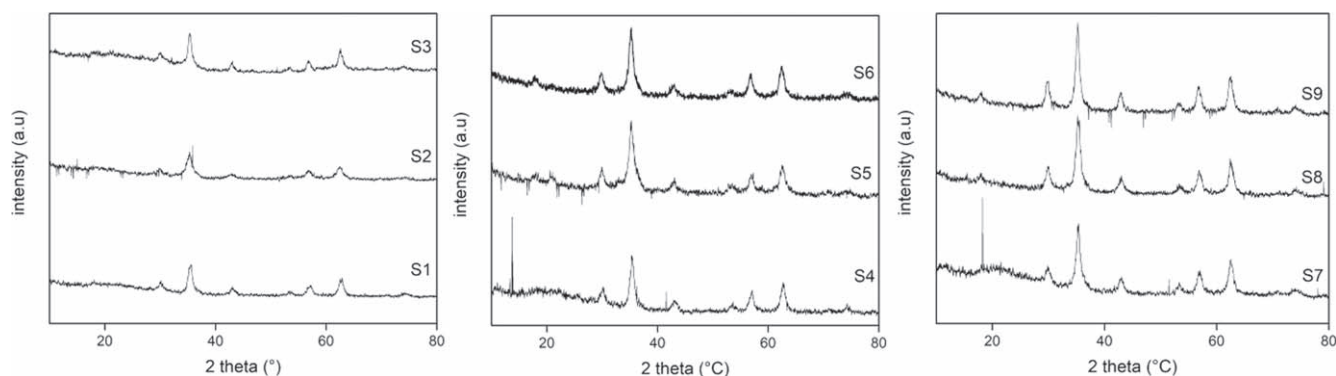
Figure 1. X-ray diffraction patterns of synthesized magnetite.

270 000×—450 000×. The software of the microscope permitted to discriminate, count, measure and perform statistical analysis of the particles. The AS and ZP of MNP (27% w/v) dispersed in a 50% v/v glycerol aqueous solution were measured using dynamic light scattering (DLS), (Zetasizer Nano-ZS, Malvern Instruments, UK), at a scattering angle of 173°. The Nano-ZS contains a 4 mW He–Ne laser (633 nm), operating with a digital correlation, model ZEN3600 and a Non-Invasive Back Scatter (NIBS®) technology. All the samples were analyzed at 25 °C. Refractive index (RI) and viscosity were 1.39 and 5 cP, respectively. Results are expressed as mean of at least three independent samples prepared under identical conditions. The software of the Zetasizer instrument used for the analysis of the data was v7.12 software (Malvern Instruments Ltd Malvern, UK). The magnetization and M_{max} of the precipitates were characterized using a Vibrating Sample Magnetometer (VSM).

3. Results and discussion

3.1. XRD analysis

Figure 1 shows the diffractograms of samples 1–9. Table 2 presents the 2θ position of the main peaks and their correspondence to the Miller indices (hkl) of their crystal lattices. Table 2 also reports the 2θ positions of reference magnetite taken from reference literature [44].

The pattern of peaks positions and intensities are well correlated with the values for magnetite reported in the literature [44]. These results indicate that all the obtained precipitates are composed of pure magnetite. No odd peaks were identified in the diffractograms. The absence of odd peaks is an evidence of the absence of any compound different than magnetite including maghemite and hematite. Maghemite and hematite are common by-products obtained during the synthesis of magnetite. The result of synthesis 1–9 is 100% magnetite despite the great variations of the studied reaction parameters. In fact, this would be a great advantage linked to the robustness required by industrial production processes.

The CS was calculated by means of the Debye–Scherrer equation [45]. Equation (2) relates the average CS to the

Table 2. XRD peaks positions in the diffraction patterns of samples 1–9.

| hkl	220	311	400	422	511	440
2θ [44]	30.1	35.46	43.09	53.46	56.99	62.58
S1	—	35.3	43.6	—	57.3	62.8
S2	30.1	35.6	43.3	53.8	57.4	62.9
S3	30.2	35.4	43.1	53.6	57.0	62.6
S4	30.7	35.7	44.4	54.5	57.7	63.3
S5	29.9	35.1	43.1	53.5	57.2	62.5
S6	29.8	35.2	42.6	53.7	56.9	62.5
S7	30.1	35.4	43.1	53.3	57.0	62.5
S8	30.0	35.2	43.1	53.3	62.4	62.4
S9	29.8	35.3	43.0	53.5	56.7	62.5

broadening of a peak in a diffraction pattern.

$$CS = k\,\lambda(\beta\cos(\theta))^{-1}. \quad (2)$$

Here, $k = 0.89$ is a constant of proportionality for integral breadth of spherical crystals, $\lambda = 1.54$ Å is the wavelength of the Cu-Kα radiation, β and θ are the broadening and the Bragg angle of the main peak, respectively. The average CS varied from a minimum of 6.9 nm corresponding to sample 2 to a maximum of 9.4 nm corresponding to sample 4. The calculated CS are reported in table 3.

3.2. TEM image analysis

Figure 2 shows, exemplary, TEM images of samples 1–9. Near spherical shape of the particles are clearly visible. This fact, justify the use of $k = 0.89$ in equation (2). The average PS varied from a minimum of 6.1 nm corresponding to sample 5 to a maximum of 9.4 nm corresponding to sample 8. The measured averages PS are also reported in table 3. Figure 3 shows the correlation between PS and CS. Interestingly, the difference between the average CS and their corresponding average PS are less than 5%. Moreover, such differences are the same when the average CS is bigger than the average PS and when the average CS are smaller than the average PS. It worth to be mentioned, that physically, the average CS have to be smaller or eventually equal to the average PS. When the CS is smaller than the PS, the particle is polycrystalline. When the CS is equal to the PS,
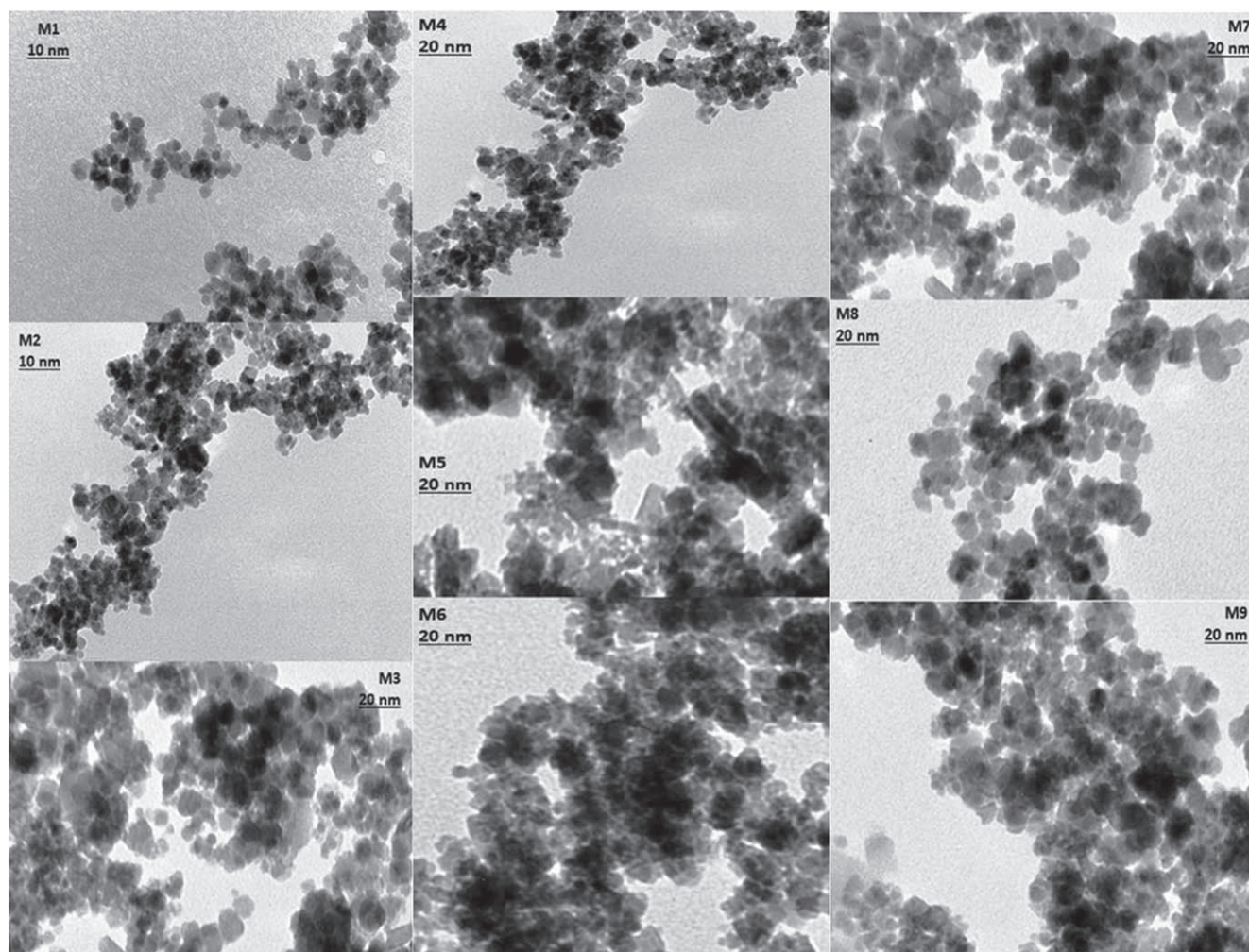
**Figure 2.** TEM images of MNP synthesized according the conditions for samples 1–9.

Table 3. Average CS, PS, AS, ZP and M_{max} of MNP.

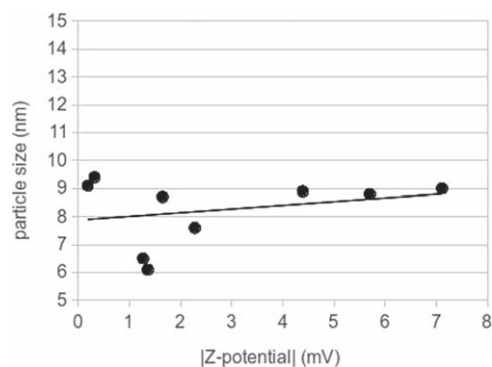| Samples	Responses				
	Crystallite size (nm)	Particle size (nm)	Aggregates size (nm)	Z-Potential (mV)	Maximum magnetization (emu g^{-1})
S1	8.7	9.0	321	−7.11	50.8
S2	6.5	6.5	801	−1.27	42.9
S3	8.4	8.7	780	−1.65	49.7
S4	9.4	9.1	740	+0.19	51.2
S5	6.0	6.1	694	+1.36	40.4
S6	7.3	7.6	672	+2.28	52.0
S7	9.1	8.9	600	+4.39	45.6
S8	8.9	9.4	800	−0.32	53.0
S9	8.5	8.8	477	+5.70	53.4

the particle is monocrystalline. It is not physically possible the CS to be bigger than the PS. Therefore, the 5% difference between the results obtained from XRD measurements and TEM measurements can be assumed as normal experimental errors. Therefore, it can be stated as preliminary conclusion that the method allowed to produce pure spherical monocrystalline MNP. Further details about the fundamentals of PS

and CS correlations can be found in the excellent work of Li *et al* [46].
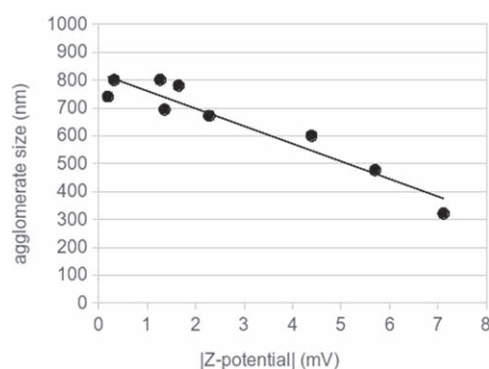
The fact the PS ≈ CS, i.e. monocrystalline nanoparticles, in all cases should also be considered an advantage for industrialization. The method here described allows to obtain spherical, pure and monocrystalline nanomagnetite.
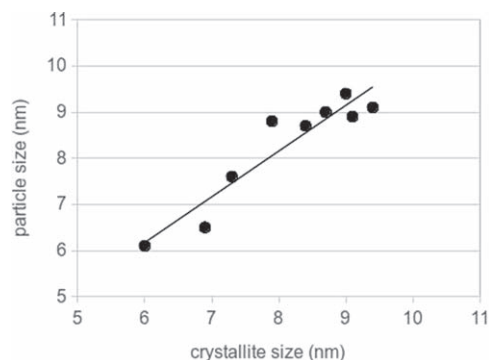
Figure 3. Correlation between PS determined by TEM and CS determined by XRD of samples 1–9.

Figure 5. Correlation between PS and ZP of MNP.

dispersion in hydrophilic or hydrophobic media or to facilitate or impair diffusion through membranes. From the industrial point of view the increase of the size of aggregates greatly facilitate the recovery of products by magnetically assisted sedimentation.

Figure 4. Correlation between AS and ZP of MNP.

3.3. DLS analysis

Figure 2 also shows the nanoparticles to be arranged in aggregates. The AS dispersed in glycerol was determined by DLS. The measured average AS are reported in table 3. Additionally, the ZP was also determined and reported in table 3. The agglomeration of particles is expected since magnetite naturally develops magnetic domains. The magnetic domains are easily self-oriented to develop attractive magnetic forces between the particles. However, the particles also develop electrostatic repulsive charges. Then, a competition between attractive magnetic forces and repulsive electrostatic forces is established. The AS is a result of the final equilibrium state of such competition.

A relationship between AS and ZP is evidenced and showed in figure 4. Here, the AS was plot against the absolute value of the ZP (|ZP|). Clearly, the smaller the AS, the higher the ZP. The biggest possible AS is about 820 nm for electrically neutral aggregates (|ZP| = 0). The smallest possible AS is defined as an aggregates composed of two nanoparticles. Such aggregates would have AS ≈ 16 nm. And they would exist at |ZP| of nearly 12.8 mV. Conversely, figure 5 shows that the PS slightly affects the ZP of resulting aggregates.

The development of electrostatic charges on the surface of MNP and aggregates of MNP may have several implications from the application point of view. Functionalization of the MNP surface can be required to facilitate their

3.4. Magnetic properties

The magnetization curves of samples 1–9, measured at 290 K with a VSM, are show in figure 6.

The absence of hysteresis loops together with the observation of practically null coercive fields are a clear indication of the superparamagnetic behavior of the MNP. Although the saturation magnetization was not reached with the maximum field applied, the M_{max} attained. The M_{max} values are reported in table 3. The obtained values of M_{max} are close to the ones reported previously for MNP of similar size [37]. The M_{max} tends to saturate, with a soft dependence on CS, as can be observed in figure 7. M_{max} increases with the increasing of the CS. This behavior can be expected for materials whose dependence of its superparamagnetic state is described by a Langevin function with an argument sensitive to the volume of the MNP [47]. This result is consisting with a inherent characteristics of pure magnetite [36, 48].

Finally, combining the results of sections 3.1, 3.2 and 3.4, it can be concluded that the precipitation method used in this contribution allowed to produce pure monocrystalline superparamagnetic spherical MNP. The robustness of the process is demonstrated. Moreover, the method allows to vary the PS and AS while maintain the magnetization properties, purity, and shape of MNP.
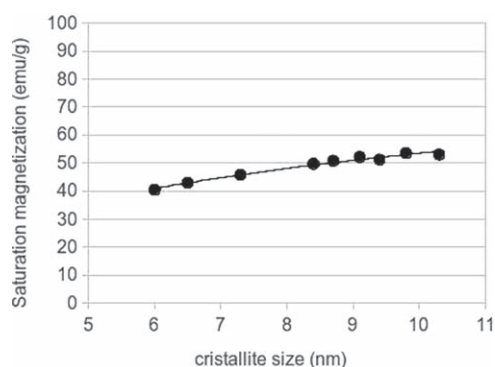
3.5. Response surface analysis and correlations

Equations (3)–(7) are own results and describe the simultaneous effects of the selected reaction parameters on the properties of MNP.

The surface responses of the PS and the AS to the stimuli of the simultaneous variation of the total iron content in the solution (*A*), the temperature (*B*), the shear rate (*C*) and the amount of NH_4OH solution (*D*) were developed as
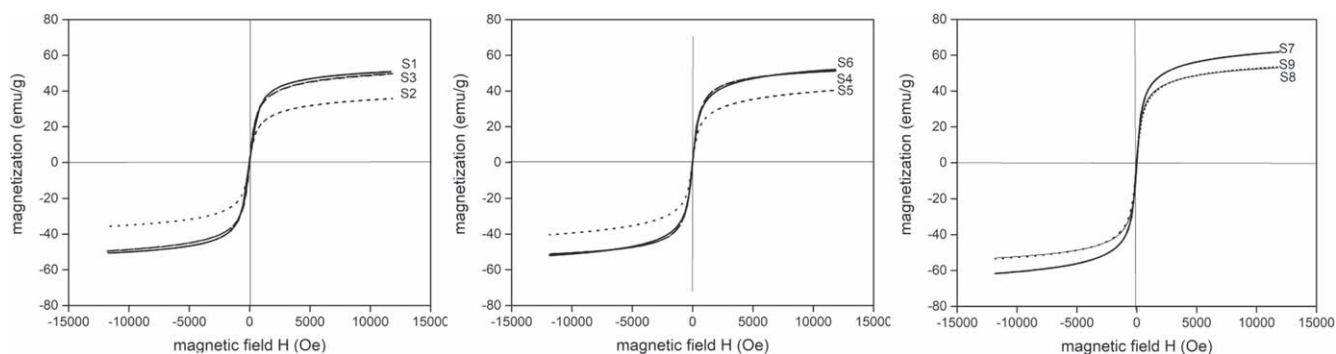
Figure 6. Magnetization curves for samples (a) 1–2–3, (b) 4–5–6 and (c) 7–8–9.

Figure 7. Correlation between M_{max} and CS of the MNP.

Figure 8. Effect of reaction temperature on the PS of MNP. Stirring speed: 500 rpm (dotted), 750 rpm (dashed) and 1000 rpm (continuous). Reaction conditions: total iron content = 0.0345 mol, NH$_4$OH solution = 35 ml.

Figure 9. Effect of total iron content on the PS of MNP. NH$_4$OH solution: 25 ml (dotted), 350 ml (dashed) and 450 ml (continuous). Reaction conditions: temperature = 50 °C, stirring speed = 750 rpm.

polynomial functions according to equations (3) and (4).

$$PS = 15.67 + 16.18A - 0.2977B - 0.005510C$$
$$+ 0.001010D + 477.0A^2 + 0.002392B^2$$
$$+ 0.000003C^2 + 0.000887D^2, \tag{3}$$

$$AS = -1646 + 40081A + 72.79B + 1.271C$$
$$+ 64.11D + 404390A^2 - 0.6580B^2$$
$$- 0.000952C^2 - 1.058D^2. \tag{4}$$

The correlations between PS and CS, M_{max} and CS and AS and ZP are shown in equations (5)–(7) and were obtained by fitting the plots in figures 3 and 4 and and 7, respectively.
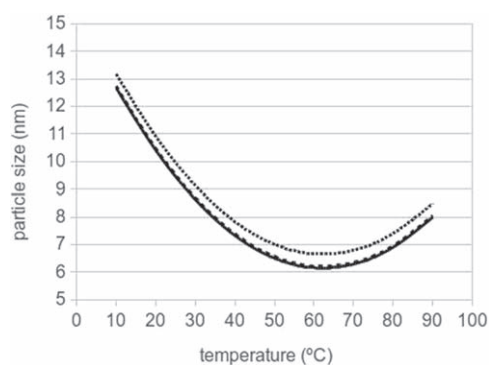
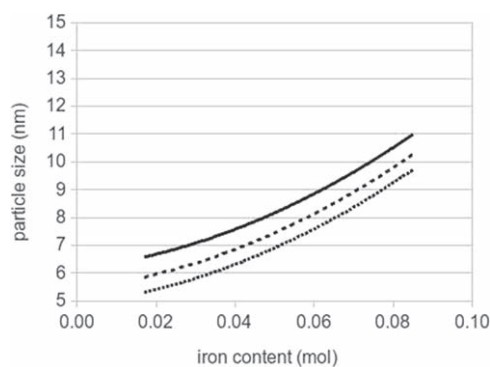$$CS = 1.01PS - 0.22 \tag{5}$$
$$AS = -63.19ZP + 824 \tag{6}$$
$$M_{max} = 24.675 \ln(CS) - 3.2927. \tag{7}$$

Equation (3) allows to visualize the effects of physical (temperature and stirring speed) and chemical (iron and NH$_4$OH contents) reaction variables on the PS of resulting MNP. Figures 8 and 9 show their corresponding 2D plots.

The temperature of precipitation plays a crucial role on the resulting PS and AS of MNP. The derivative of equation (3) permits to find the minimum PS. The minimum PS occurs when the co-precipitation reaction is carried out at $T = 62.2$ °C. Higher and lower co-precipitation temperatures result in higher PS. This behavior is explained by the nucleation theory of the chemical co-precipitation process [26, 34]. On the one hand, the higher the temperature, the faster the mobility of species and the higher the rate of grow

of nuclei. Additionally, the higher the temperature, the greater the tendency to dissolution of the small nuclei and only the big ones tend to grow. As consequence, the higher the temperature, the higher the PS. On the other hand, the lower temperature, the bigger the critical size of nuclei and the higher is the final PS.

Equation (4) allows to visualize the effects of physical (temperature and stirring speed) and chemical (iron and NH4OH contents) reaction variables on the AS of resulting MNP. Figures 10 and 11 show their corresponding 2D plots.

Figure 10. Effect of reaction temperature on the AS of MNP. Stirring speed: 500 rpm (dotted), 750 rpm (dashed) and 1000 rpm (continuous). Reaction conditions: total iron content = 0.0345 mol, NH_4OH solution = 35 ml.
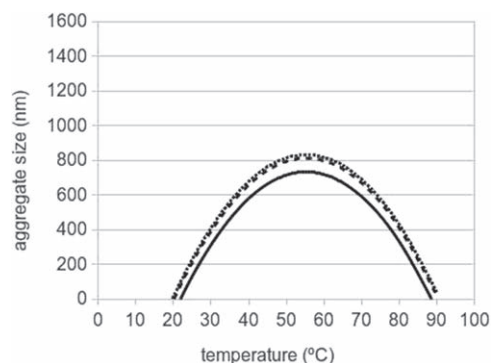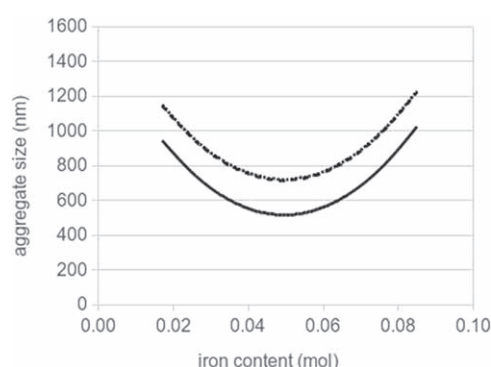

Figure 11. Effect of total iron content on the AS of MNP. NH_4OH solution: 25 ml (dotted), 35 ml (dashed) and 45 ml (continuous). Reaction conditions: temperature = 50 °C, stirring speed = 750 rpm.

The derivative of equation (4) permits to find the maximum AS. The maximum AS occurs when the co-precipitation reaction is carried out at $T = 55.3$ °C. The co-precipitation reaction carried out at $T = 55.3$ °C and 500 rpm gives as result MNP with AS ~ 800 nm and ZP ~ 0 mV. In those conditions the surface of the resulting MNP are electrically neutral when dispersed in glycerol. As consequence, the nanoparticles aggregate due to the absence of repulsive electrostatic forces and the inherent presence of attractive magnetic forces developed by the magnetic domains of magnetite crystals.

The mixing degree seems to have a small effect on PS and AS. A decrease of PS and AS of less than 10% is observed when the stirring speed is increased from 500 to 1000 rpm in all the range of co-precipitation temperatures. The slight decrease of PS with the increase of the rpm is explained in terms of the finer dispersion of nuclei promoted by the higher shear rate of the system [33].

The PS increases monotonically with the increase of the amount of iron and ammonium in the solution. The higher the concentration of both reactants, the bigger the PS of resulting MNP. However, the concentration of iron and ammonium in the co-precipitation medium seems to have differential effects on the electrostatic nature of the surface

of resulting MNP. On the one hand, the higher the ammonium concentration in the co-precipitation medium the higher the surface charge of resulting MNP and thus the higher the electrostatic repulsive forces between them and the smaller AS. On the other hand, a co-precipitation medium with total iron content of 0.05 mol results in minimal AS of MNP. Total iron content higher than 0.05 mol tend to generate negatively charged MNP. Conversely, total iron content lower than 0.05 mol tend to generate positively charged MNP. In both cases, the resulting AS is decreased by the action of repulsive electrostatic forces due to the development of negative or positive charges on the surface of resulting MNP, respectively.

4. Conclusions

The cross-dependencies of main physical and chemical reaction parameters of co-precipitation synthesis on the resulting properties of MNP were investigated. A set of equations in the form of 4D surfaces was developed. The set of equations relates the temperature, the degree of mixing, the total iron content and the amount of ammonium hydroxide used for pH adjustment during the co-precipitation reaction with the CS, PS and M_{max} of MNP and the ZP and AS of their corresponding aggregates. The results were discussed in terms of crystal nucleation and growth theories. The synthesis protocol results in pure monocrystalline superparamagnetic spherical magnetite nanoparticles. The 4D surface response set of equations permits to predict precisely the properties of resulting MNP by adjusting the main physical and chemical reaction conditions. The integrated set of equations (3)–(7) models a prediction of the properties of MNP using as input data the values corresponding to the main reaction parameters. This integrated set of equations can be useful to monitor, control and correct on real time basis the path of the co-precipitation process for industrial fabrication of MNP.

Acknowledgments

Conflicts of interest

There are no conflicts to declare.

ORCID iDs

Carlos Acha ⓘ https://orcid.org/0000-0002-8650-4343
Ignacio Rintoul ⓘ https://orcid.org/0000-0002-0766-9554

References

[1] Alphandéry E 2019 Biodistribution and targeting properties of iron oxide nanoparticles for treatments of cancer and iron anemia disease *Nanotoxicology* **13** 573–96

[2] Palanisamy S and Wang Y M 2019 Superparamagnetic iron oxide nanoparticulate system: synthesis, targeting, drug delivery and therapy in cancer *Dalton Trans.* **48** 9490–515

[3] Sangaiya P and Jayaprakash R 2018 A review on iron oxide nanoparticles and their biomedical applications *J. Supercond. Nov. Magn.* **31** 3397–413

[4] Zhang H *et al* 2018 Magnetic nanoparticles based cancer therapy: current status and applications *Sci. China Life Sci.* **61** 400–14

[5] Song C, Sun W, Xiao Y and Shi X 2019 Ultrasmall iron oxide nanoparticles: synthesis, surface modification, assembly, and biomedical applications *Drug Discov. Today* **24** 835–44

[6] Deng Y, Xu A, Yu Y, Fu C and Liang G 2019 Biomedical applications of fluorescent and magnetic resonance imaging dual-modality probes *ChemBioChem* **20** 499–510

[7] Xie L, Jin W, Chen H and Zhang Q 2019 Superparamagnetic iron oxide nanoparticles for cancer diagnosis and therapy *J. Biomed. Nanotechnol.* **15** 215–35

[8] Anderson S D, Gwenin V V and Gwenin C D 2019 Magnetic functionalized nanoparticles for biomedical, drug delivery and imaging applications *Nanoscale Res. Lett.* **14** 188

[9] Hu Y, Mignani S, Majoral J P, Shen M and Shi X 2018 Construction of iron oxide nanoparticle-based hybrid platforms for tumor imaging and therapy *Chem. Soc. Rev.* **47** 1874–900

[10] Rodrigues G R *et al* 2019 Antimicrobial magnetic nanoparticles based-therapies for controlling infectious diseases *Int. J. Pharm.* **555** 356–67

[11] de Toledo L D A S, Rosseto H C and Bruschi M L 2018 Iron oxide magnetic nanoparticles as antimicrobials for therapeutics *Pharm. Dev. Technol.* **23** 316–23

[12] Vangijzegem T, Stanicki D and Laurent S 2019 Magnetic iron oxide nanoparticles for drug delivery: applications and characteristics *Expert Opin. Drug Del.* **16** 69–78

[13] Xiong F, Huang S and Gu N 2018 Magnetic nanoparticles: recent developments in drug delivery system *Drug Dev. Ind. Pharm.* **44** 697–706

[14] El-Boubbou K 2018 Magnetic iron oxide nanoparticles as drug carriers: Preparation, conjugation and delivery *Nanomedicine* **13** 929–52

[15] Das P, Colombo M and Prosperi D 2019 Recent advances in magnetic fluid hyperthermia for cancer therapy *Colloids Surf.* B **174** 42–55

[16] Noqta O A, Aziz A A, Usman I A and Bououdina M 2019 Recent advances in iron oxide nanoparticles (IONPs): synthesis and surface modification for biomedical applications *J. Supercond. Nov. Magn.* **32** 779–95

[17] Ahmad F, Ashraf N, Ashraf T, Zhou R B and Yin D C 2019 Biological synthesis of metallic nanoparticles (MNPs) by plants and microbes: their cellular uptake, biocompatibility, and biomedical applications *Appl. Microbiol. Biotechnol.* **103** 2913–35

[18] Bhateria R and Singh R 2019 A review on nanotechnological application of magnetic iron oxides for heavy metal removal *J. Water Process Eng.* **31** 100845

[19] Wong J K H, Tan H K, Lau S Y, Yap P S and Danquah M K 2019 Potential and challenges of enzyme incorporated nanotechnology in dye wastewater treatment: a review *J. Environ. Chem. Eng.* **7** 103261

[20] Song D, Yang R, Long F and Zhu A 2019 Applications of magnetic nanoparticles in surface-enhanced Raman scattering (SERS) detection of environmental pollutants *J. Environ. Sci. China* **80** 14–34

[21] Horszczaruk E 2019 Properties of cement-based composites modified with magnetite nanoparticles: a review *Materials* **12** 326–60

[22] Kalantari F, Ramazani A and Heravi M R P 2019 Recent advances in the applications of hybrid magnetic nanomaterials as magnetically retrievable nanocatalysts *Curr. Org. Chem.* **23** 136–63

[23] Ma J, Guo X, Yan Y, Xue H and Pang H 2018 FeOx -based materials for electrochemical energy storage *Adv. Sci.* **5** 1700986

[24] Patel S K S, Lee J K and Kalia V C 2018 Nanoparticles in biological hydrogen production: an overview *Indian J. Microbiol.* **58** 8–18

[25] Vayssières L, Chanéac C, Tronc E and Jolivet J P 1998 Size tailoring of magnetite particles formed by aqueous precipitation: an example of thermodynamic stability of nanometric oxide particles *J. Colloid Interface Sci.* **205** 205–12

[26] Cushing B L, Kolesnichenko V L and O'Connor C J 2004 Recent advances in the liquid-phase syntheses of inorganic nanoparticles *Chem. Rev.* **104** 3893–946

[27] Laurent S, Forge D, Port M, Roch A, Robic C, Vander Elst L and Muller R N 2008 Magnetic iron oxide nanoparticles: synthesis, stabilization, vectorization, physicochemical characterizations, and biological applications *Chem. Rev.* **108** 2064–110

[28] Baumgartner J, Dey A, Bomans P H H, Le Coadou C, Fratzl P, Nico A J M, Sommerdijk N A J M and Faivre D 2013 Nucleation and growth of magnetite from solution *Nat. Mater.* **12** 310–4

[29] Fang M, Ström V, Olsson R T, Belova L and Rao K V 2012 Particle size and magnetic properties dependence on growth temperature for rapid mixed co-precipitated magnetite nanoparticles *Nanotechnology* **23** 145601–10

[30] Mahdavi M, Ahmad M B, Haron M J, Namvar F, Nadi B, Rahman M Z A and Amin J 2013 Synthesis, surface modification and characterisation of biocompatible magnetic iron oxide nanoparticles for biomedical applications *Molecules* **18** 7533–48

[31] Sun J, Zhou S, Hou P, Yang Y, Weng J, Li X and Li M 2006 Synthesis and characterization of biocompatible Fe_3O_4 nanoparticles *J. Biomed. Mater. Res.* A **10** 333–41

[32] Chia C H, Zakaria S, Farahiyan R, Khong L T, Nguyen K L, Abdullah M and Ahmad S 2008 Size-controlled synthesis and characterization of Fe_3O_4 nanoparticles by chemical coprecipitation method *Sains Malaysiana* **37** 389–94

[33] Sunaryono S, Ahmad T, Mashuri M, Suminar P, Zainuri M, Triwikantoro T and Darminto D 2015 Various magnetic properties of magnetite nanoparticles synthesized from iron-sands by coprecipitation method at room temperature *Mater. Sci. Forum* **827** 229–34

[34] Babes L, Denizot B, Tanguy G, Le Jeune J J and Jallet P 1999 Synthesis of iron oxide nanoparticles used as MRI contrast agents: a parametric study *J. Colloid Interface Sci.* **212** 474- 482

[35] Nedkov I, Kolev S, Zadro K, Krezhov K and Merodiiska T 2004 Crystalline anisotropy and cation distribution in nanosized quasi-spherical ferroxide particles *J. Magn. Magn. Mater.* **272–276** E1175–6

[36] Mascolo M C, Pei Y and Ring T A 2013 Room temperature co-precipitation synthesis of magnetite nanoparticles in a large pH window with different bases *Materials* **6** 5549–67

[37] Goya G F, Berquó T S, Fonseca F C and Morales M P 2003 Static and dynamic magnetic properties of spherical magnetite nanoparticles *J. Appl. Phys.* **94** 3520–8

[38] Wang B, Wei Q and Qu S 2013 Synthesis and characterization of uniform and crystalline magnetite nanoparticles via oxidation-precipitation and modified co-precipitation methods *Int. J. Electrochem. Sci.* **8** 3786–93

[39] Mahmed N, Heczko O, Söderberg O and Hannula S P 2011 Room temperature synthesis of magnetite ($Fe_{3-\delta}O_4$) nanoparticles by a simple reverse co-precipitation Method *IOP Conf. Ser. Mater. Sci. Eng.* **18** 032020

[40] Dieter G E and Schmidt L C 2013 *Engineering Design* 5th edn (New York: McGraw-Hill International Editions) Ch 15

[41] Daza Agudelo J I 2018 Development of drug-controlled release PVA hydrogel composites triggered by radiofrequency external stimuli *Doctoral Thesis* Universidad Nacional del Litoral and Ulm University

[42] Daza Agudelo J I, Badano J M and Rintoul I 2018 Kinetics and thermodynamics of swelling and dissolution of PVA gels obtained by freeze-thaw technique *Mater. Chem. Phys.* **216** 14–21

[43] Quiroga A, Marzocchi V and Rintoul I 2016 Influence of wood treatments on mechanical properties of woodecement composites and of Populus Euroamericana wood fibers *Composites* B **84** 25–32

[44] Haavik C, Stolen S, Fjellvag H, Hanfland M and Hausermann D 2000 Equation of state of magnetite and its high-pressure modification: thermodynamics of the Fe–O system at high pressure *Am. Mineral.* **84** 514–23

[45] Langford J I and Wilson A 1978 Scherrer after sixty years: a survey and some new results in the determination of crystallite size *J. Appl. Crystallogr.* **11** 102–13

[46] Li Q, Kartikowati C W, Horie S, Ogi T, Iwaki T and Okuyama K 2017 Correlation between particle size/domain structure and magnetic properties of highly crystalline Fe_3O_4 nanoparticles *Sci. Rep.* **7** 1–4

[47] Cullity B D and Graham C D 2009 *Introduction to Magnetic Materials* 2nd edn (New York: Wiley) ch 11

[48] Morales M P, Andres-Verges M, Veintemillas-Verdaguer S, Montero M I and Serna C J 1999 Structural effects on the magnetic properties of gamma-Fe_2O_3 nanoparticles *J. Magn. Magn. Mater.* **203** 146–8